Journal of Nuclear Materials 496 (2017) 301–312

Contents lists available at ScienceDirect

Journal of Nuclear Materials

journal homepage: www.elsevier.com/locate/jnucmat

The role of hydrogen in zirconium alloy corrosion

B. Ensor [a, b, *], A.M. Lucente [b], M.J. Frederick [b], J. Sutliff [b], A.T. Motta [a]

[a] Department of Mechanical and Nuclear Engineering, The Pennsylvania State University, University Park, PA 16802, USA
[b] Knolls Atomic Power Laboratory, Naval Nuclear Laboratory, Schenectady, NY 12309, USA

HIGHLIGHTS

- Systematic study of the effects of H concentration on oxide growth in Zircaloy-4.
- The formation of hydrides is associated with accelerated zirconium alloy corrosion.
- H concentrations above the TSS leads to earlier periodic oxide transitions.
- Advanced corrosion into the metal where hydrides precipitated near the MOI.
- Thought that local hardening of the metal matrix leads to earlier oxide transitions.

GRAPHICAL ABSTRACT

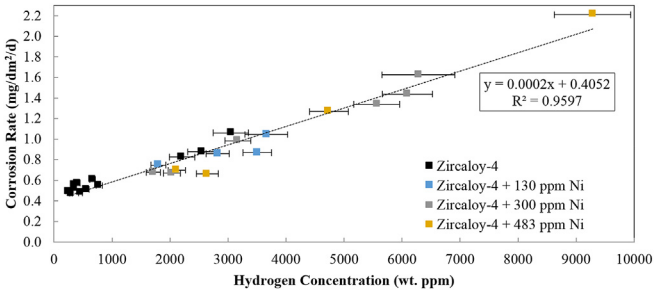

ARTICLE INFO

Article history:
Received 14 June 2017
Received in revised form
17 August 2017
Accepted 25 August 2017
Available online 27 September 2017

Keywords:
Zirconium alloy
Zircaloy-4
Corrosion
Hydrogen
Terminal solid solubility
Autoclave

ABSTRACT

Hydrogen enters zirconium metal as a result of the corrosion process and forms hydrides when present in quantities above the solubility limit at a given temperature. Zircaloy-4 coupons of different thicknesses (0.4 mm-2.3 mm) but identical chemistry and processing were corroded in autoclave at 360 °C for various times up to 2800 days. Coupons were periodically removed and weighed to determine weight gain, which allows follow of the corrosion kinetics. Coupon thickness differences resulted in different volumetric concentrations of hydrogen, as quantified using hot vacuum extraction. The thinnest coupons, having the highest concentration of hydrogen, demonstrated acceleration in their corrosion kinetics and shorter transition times when compared to thicker coupons. Furthermore, it was seen that the post-transition corrosion rate was increased with increasing hydrogen concentration. Corrosion rates increased only after the terminal solid solubility (TSS) was exceeded for hydrogen in Zircaloy-4 at 360 °C. Therefore, it is hypothesized that the corrosion acceleration is caused by the formation of hydrides. Scanning electron microscope (SEM) examinations of fractured oxide layers demonstrate the oxide morphology changed with hydrogen content, with more equiaxed oxide grains in the high hydrogen samples than in those with lower hydrogen content. Additionally, locations of advanced oxide growth were correlated with locations of hydrides in the metal. A hypothesis is proposed to explain the accelerated corrosion due to the presence of the hydrides, namely that the metal, locally, is less able to accommodate oxide growth stresses and this leads to earlier loss of oxide protectiveness in the form of more frequent oxide kinetic transitions.

1. Introduction and literature review

Despite having been the subject of extensive research for

* Corresponding author. PO Box 1072, Mail Stop 102, Schenectady, NY 12301, USA.
E-mail address: brendan.ensor@gmail.com (B. Ensor).

https://doi.org/10.1016/j.jnucmat.2017.08.046
0022-3115/

decades, the corrosion of zirconium alloys in nuclear power plants is still not fully understood [1]. As the metal initially rapidly corrodes in the high temperature water present in a nuclear reactor core, the oxide layer that forms is protective and slows down further oxidation. This protective oxide layer is constituted of mostly monoclinic phase zirconium dioxide with some tetragonal phase by the following reaction of Zr metal:

$$Zr_{metal} + 2H_2O_{liquid} \rightarrow ZrO_2 + 2H_2 \quad (1)$$

The kinetics of this oxidation reaction are well described by the power law shown in Equation (2),

$$W = At^n \quad (2)$$

where W is the weight gain, t is the exposure time, A is a constant, and n is an exponent which for autoclave corrosion at 360 °C typically ranges anywhere from 0.2 to 0.5 depending on the alloy [1]. Eventually, the oxide kinetics accelerate during what is known as transition, as depicted in Fig. 1.

Hydrogen can play an important role in the corrosion process of Zr alloys. Because of conservation of mass and charge balance, the oxidation reaction has to be balanced by a reduction reaction, which is generally the hydrogen evolution reaction. Because only a fraction of the hydrogen that is produced by this reaction enters the metal, hydrogen pickup is typically quantified through the hydrogen pickup fraction [2–4]. The hydrogen that enters the cladding material is found in solid solution as long as its concentration remains below the terminal solid solubility (TSS) for hydrogen of the zirconium alloy [2,5–10]. The TSS increases with temperature, such that negligible hydrogen can be dissolved into the metal at room temperature but up to ~120–140 wt ppm can be dissolved at 360 °C, depending on the alloy [2,5–10].

The terminal solid solubility for hydride precipitation (TSS_p) during cooling is different from the terminal solid solubility for hydride dissolution during heating (TSS_d) [5,11]. The difference between these two concentrations is important for many applications, but in the experiment described herein, the quantity of interest is the TSS_d. This is because during autoclave corrosion experiments, the autoclave is cooled down relatively frequently to weigh the samples. During the cool down to room temperature, all of the hydrogen is precipitated out as hydrides. Upon reheating, the hydrides dissolve into the matrix, but only up to the TSS_d. For simplicity, in the remainder of this paper, the relevant concentration limit, TSS_d, will be referred to as the TSS.

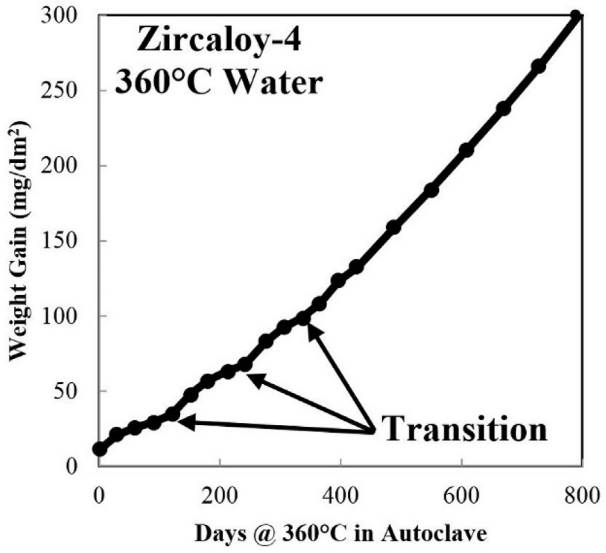

Fig. 1. Weight gain (which is directly correlated with oxide thickness) versus time of a Zircaloy-4 coupon corroded in 360 °C water in autoclave illustrating the cyclic nature of oxide growth and transition cycles.

Fig. 2 shows an example of oxide thickness as a function of burnup for Zircaloy-4 in PWRs and demonstrates the commonly observed accelerated corrosion in commercial reactor claddings subject to high fuel burnup [5,12–16]. One hypothesis to explain this accelerated corrosion is that it is caused by hydride formation at high burnup [12,13,15]. Other factors have been correlated to accelerated in-reactor corrosion, including dislocation formation and accumulation, precipitate amorphization and dissolution, water chemistry (such as the addition of Li), and irradiation growth [12]. However, the observed corrosion rate change at high burnup should be correlated to some parameter that changes at a given exposure, such as hydride formation. Irradiation dissolution and precipitate amorphization, the formation of dislocation loops, water chemistry, and gamma irradiation operate continuously since the beginning of irradiation and in the case of the latter two are present at all times during reactor operation with little change [17]. Since hydride formation can be correlated to accelerated corrosion, it is important to understand the magnitude and onset of this effect, if any, on corrosion resistance of zirconium alloys that are exposed to water for a sufficient duration to cause hydride precipitation.

Initial studies focused on formation of hydrides at the metal-oxide interface (MOI) of Zircaloy-4 [13]. It is known that hydrogen migrates towards regions of high stress and those that are coldest [2,5,13,18,19]. Since in a fuel rod the metal-oxide interface is the coldest location of the metal (farthest from the heat flux of inner fuel pellets and closest to coolant) the hydrogen accumulates there, which leads to hydride formation [13]. This has been verified in many studies [5,18,19].

To study the effect of hydrides on corrosion, researchers performed tests on zirconium alloy samples charged with hydrogen prior to autoclave exposure [12,14,20,21]. Kido demonstrated uniform corrosion acceleration caused by hydrogen in 360 °C water with pre-charged zirconium alloy samples [21]. Results from Blat and Noel from autoclave corrosion tests (under various conditions, including 360 °C primary water, 360 °C heavy water, 400 °C steam, and in furnace with air at 400 °C) on Zircaloy-4 cladding precharged with hydrogen using both gaseous and cathodic charging techniques similarly showed accelerated corrosion for samples with more hydrides [14,20]. Of note was that no acceleration of the corrosion kinetics in the pre-transition regime was observed by Kido in materials with higher initial hydrogen concentration [12]. Blat and Noel showed that a thick outer hydride layer (created by cathodic hydrogen charging) was correlated to a significant increase in corrosion as measured by weight gain [14]. Overall, these initial studies indicate that the accumulation of hydrogen can have a deleterious effect on corrosion.

Autoclave tests at 340 °C (water), 360 °C (water), and 400 °C (steam) of Zircaloy-4 tube specimens pre-charged with hydrogen from ~100 to 3000 wt ppm showed that the corrosion temperature affected the onset of accelerated corrosion due to hydrogen, and that this onset correlated with the TSS for those particular temperatures [12]. Once the TSS_P was reached, the corrosion accelerated, as shown in Fig. 3 showing post-transition corrosion rate as a function of hydrogen concentration from the work performed by Kido et al. [12].

A number of possibilities for the mechanism of hydrogen-based accelerated corrosion have been proposed including:

- Faster corrosion of the zirconium hydride as compared to the Zr matrix [14].

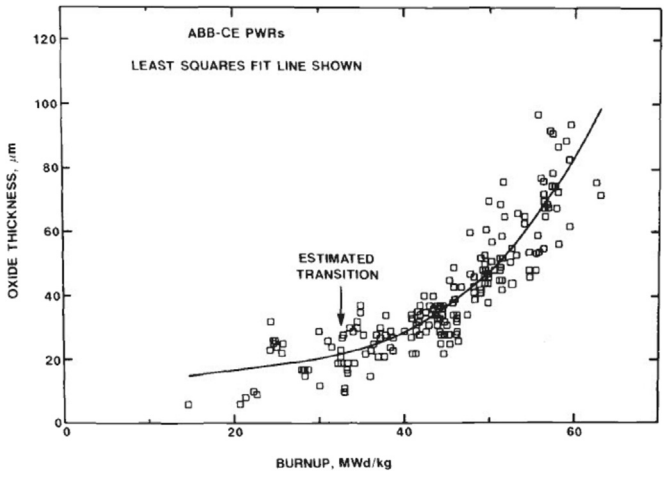

Fig. 2. Examples of accelerated corrosion of Zircaloy-4 in high burnup material, showing that at high burnups, corrosion enters an accelerated regime [13].

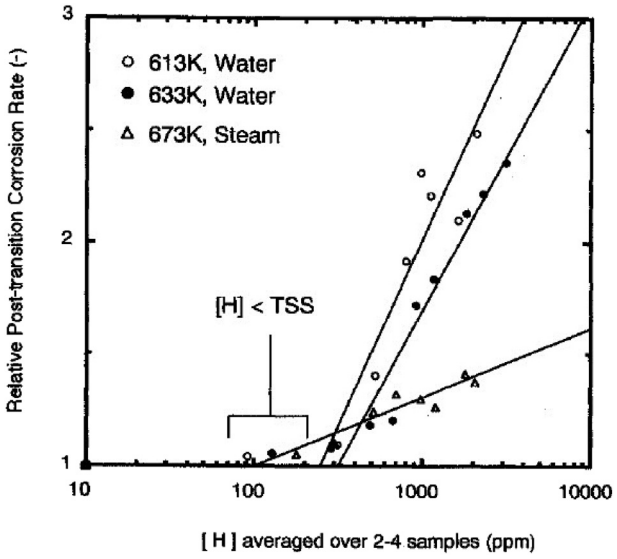

Fig. 3. Post-transition corrosion rate in zirconium alloys as a function of initial hydrogen concentration in various corrosion media showing similar shapes as those in Fig. 2 (oxide thickness vs. fuel burnup) [12].

- Different, less protective, oxide microstructure grown on the metal caused by the presence of hydrogen [14].
- The formation of hydrides affects local stress at the metal-oxide interface, thus increasing the frequency of the periodic transitions [15,22].

While secondary ion mass spectrometry (SIMS) and transmission electron microscopy (TEM) studies have shown faster diffusion of oxygen (^{18}O) in samples with a dense hydride layer (formed from pre-charging) than those where no hydride layer was present [15], it is not clear how diffusion of oxygen through hydrides or metal can change the corrosion rate, particularly since the rate-limiting step requires transport through the oxide layer already present. TEM observations did show that more equiaxed grains were observed in the oxide formed on a pre-hydrided sample than in a non-hydrided sample [15]. However, an equiaxed oxide structure is often associated with accelerated corrosion under a variety of conditions and it could be a *consequence* of a higher corrosion rate rather than a cause of it [23,24].

A mechanical response to the formation of hydrides could be the cause of the accelerated corrosion rate. It was observed that the periodicity of the cracks from kinetic transitions became more closely spaced with increased hydrogen content and the authors hypothesized that stress changes from the formation of hydrides could play a role in the increased corrosion rate [20]. This could mean that the formation of hydrides near the metal-oxide interface changes the local mechanical properties of the metal in that location. If the metal becomes harder and is less able to accommodate oxide growth stresses, a critical stress at the metal-oxide interface could be reached sooner, leading to an earlier, local kinetic transition in the oxide.

One concern that arises from many of the experiments described above is whether samples pre-charged with hydrogen accurately represent the behavior of these alloys as they corrode, since hydrogen (not including trace hydrogen present in the ingots) normally only accumulates as a result of the corrosion reaction. In this paper, the comparison of identical samples with various thicknesses over a long exposure allows for an evaluation of hydrogen effects without the potential confounding effects of pre-hydriding. This is because the differences in hydrogen content are solely due to differences in surface area to volume ratio among the specimens. Hydrogen concentration analyses performed using LECO measurements provide an accurate measure of hydrogen concentration evolution. Using these two points, the objective of this paper is to perform a systematic determination of the presence and onset of hydrogen-accelerated corrosion. This fits into a larger study on the causes of unstable oxide growth in zirconium and zirconium alloys [25].

2. Materials and experimental testing

The autoclave-coupon thickness variation experiment discussed herein used recrystallized, alpha-annealed Zircaloy-4 from two ingots (with sample IDs of 1000xx and 560xx). These coupons were processed in an identical manner to previously reported Zircaloy-4 samples, that is warm-rolled and annealed resulting in an equiaxed alpha-Zr grain structure and can be characterized by a cumulative annealing parameter, ΣA, of ~1×10^{-16} (with a Q value of 40,000) [26–29]. Precipitates were characterized as being mostly hexagonal (C14) $Zr(Fe,Cr)_2$ Laves Phase precipitates with a range of sizes from 0.2 to 0.4 μm and an average size of 0.24 μm [30,31]. Coupons from ingots of Zircaloy-4 with additions of 130, 300, and 480 ppm Ni were also tested (sample IDs of 2010xx, 2020xx, and 2030xx, respectively) and were processed in an identical manner to the Zircaloy-4. The compositions of the samples tested in this work are listed in Table 1. Coupons from the two Zircaloy-4 ingots were machined to dimensions of 2.54 cm wide by 5.08 cm in length with five nominal thicknesses: 0.4 mm, 1.0 mm, 1.7 mm, and 2.3 mm. Precise measurements of the final dimensions (accurate to 0.01 mm) and initial weight (accurate to 0.01 mg) were recorded for each coupon. Samples underwent pickling in HNO_3/HF as a final surface preparation step. All samples were tested in the same static autoclave at 360 °C and 18.57 MPa. After each exposure time the

Table 1
Compositions for zirconium alloy samples tested in autoclave with 360 °C water.

Coupon ID	Sn	Fe	Cr	Ni	Zr
1000xx	1.58%	0.21%	0.12%	–	bal.
560xx	1.51%	0.21%	0.10%	–	bal.
2010xx	1.62%	0.22%	0.11%	130 ppm	bal.
2020xx	1.60%	0.22%	0.11%	300 ppm	bal.
2030xx	1.59%	0.21%	0.11%	483 ppm	bal.

Table 2
Samples of Zircaloy-4 and other alloys from Table 1 chosen for H LECO testing with measured H content.

Coupon ID	Sample Thickness (mm)	Exposure Time (days)	Oxide Thickness (μm)	H Content (wt. ppm)
56009	2.28	3	0.8	12.5
56010	2.29	120	2.3	16.2
100011	2.14	242	4.4	43.5
56012	2.26	397	8.4	68.5
100013	2.17	1031	25.8	252
56015	2.29	1504	43.8	352
100016	2.13	1804	52.9	356
56017	1.65	3	0.6	10.5
56018	1.65	120	2.1	21.5
56019	1.65	242	4.7	44.5
56020	1.61	397	8.4	91.5
56021	1.63	1031	27.7	296
100024	1.65	1504	42.1	406
56024	1.58	1804	54.7	553
56025	1.03	3	0.9	27
100027	1.04	242	4.4	84.5
100028	0.93	397	8.1	146
100029	0.96	1031	27.2	458
56029	1.02	1504	45.4	664
100032	1.02	1804	54.9	779
56035	0.39	3	0.7	33
56036	0.39	120	2.1	45.1
56037	0.36	242	5.0	222
100036	0.38	397	8.4	369
56042	0.36	1504	57.3	2210
56041	0.38	1804	72.9	2560
56040	0.38	2204	99.4	3050
201037	0.37	1031	34.0	1800
201039	0.34	1504	65.1	2820
201040	0.38	1804	79.4	3505
201038	0.37	2204	109.5	3660
202030	0.99	1504	52.5	1715
202032	1.04	1804	66.0	2035
202037	0.38	1031	44.5	3170
202040	0.36	1504	84.9	5565
202038	0.38	1804	111.6	6280
202039	0.39	1804	107.0	6095
203031	1.01	1504	54.0	2115
203032	0.97	1804	68.4	2645
203037	0.36	1031	54.3	4740
203039	0.37	1504	111.5	9285

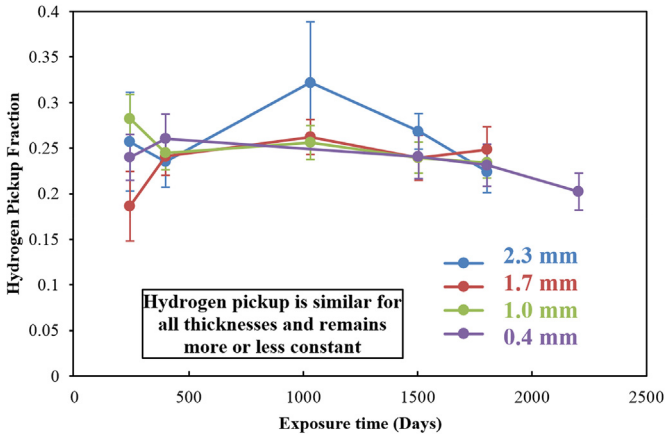

Fig. 4. Hydrogen pickup fraction as a function of corrosion time for Zircaloy-4 360 °C autoclave corrosion coupons.

samples were removed, cleaned, dried, and weighed before being returned to the autoclave for the next corrosion period. The first period was 3 days, the next 14 were ~30 days each, followed by measurement every ~60 days, and eventually ~100 days.

Samples were systematically chosen for hydrogen concentration testing as a function of coupon thickness and exposure time, as shown in Table 2. Because of the difference in thicknesses, the hydrogen concentrations are much higher in the thinner samples.

Oxide thicknesses are calculated based on the approximate conversion of 15 mg/dm^2 = 1 μm. Twenty-two of the samples were cut into 2.54 mm × 2.54 mm squares and five samples (100016, 100024, 56024, 56010, and 56036) were cut into different size squares (sized to reach the required mass of 0.25–0.5 g) for hot vacuum extraction testing of hydrogen concentration using a LECO Model RHEN602. All tests were done on duplicate pieces of the same sample except for 6 samples (56035, 56037, 100036, 56042, 56041, and 56040) for which there was insufficient material. Measurement uncertainty was 10% of the measured value or 10 wt ppm, whichever was greater. Calculated overall hydrogen pickup fraction was approximately the same (between 20 and 30%) for the Zircaloy-4 material, and did not change appreciably during exposure. Hydrogen pickup was not measured for the alloys with Ni additions. Fig. 4 shows hydrogen pickup fraction, as defined in Ref. [4], as a function of exposure time.

Samples were chosen for fatigue fracture testing and imaging

Table 3
Samples chosen for fracture testing and SEM imaging.

Coupon ID	Thickness	Exposure Time	Oxide Thickness	Estimated H Conc.
100014	2.17 mm	1504 days	42.0 μm	350 wt ppm
100020	1.65 mm	397 days	7.8 μm	90 wt ppm
100032	1.02 mm	1804 days	54.9 μm	*779 wt ppm (actual)*
56030	1.03 mm	397 days	8.5 μm	150 wt ppm
100039	0.38 mm	1804 days	71.6 μm	2560 wt ppm
56038	0.39 mm	397 days	8.7 μm	370 wt ppm

The italicized hydrogen concentration is an actual measurement of hydrogen concentration, while the remaining samples only have estimated hydrogen concentrations.

based on the amount of time they were exposed to the corrosion environment and coupon thickness as shown in Table 3. This offered a range of hydrogen concentrations for examination.

Specimens were fatigued until fracture using the three-point bend formulas that are available in both ASTM Standards E399 (Standard Test Method for Linear-Elastic Plane-Strain Fracture Toughness K_{IC} of Metallic Materials) and E1820 (Standard Test Method for Measurement of Fracture Toughness) [32,33]. Specimens in Table 3 had a range of ductility but they all fractured within a day, depending on frequency and force range applied. Testing was done with an MTS® table top 'A' frame with a maximum capacity of 2268 kgf in tension and compression. After fracture, samples were gold-coated and examined using a Zeiss Auriga 60 scanning electron microscope (SEM) to determine morphology of the oxide grains.

3. Results

Weight gain results for the Zircaloy-4 samples corroded at 360 °C in a static autoclave with high-purity deaerated water are shown in Fig. 5. Fig. 5 includes results from 0.4 mm samples (purple), 1.0 mm samples (green), 1.7 mm samples (red), and 2.3 mm samples (blue). Fig. 5 illustrates that the thinnest coupons showed the highest weight gain, followed by the next thinnest set of samples, whereas the two thickest set of coupons had the lowest weight gain. The results of the LECO hydrogen hot vacuum extraction of the samples listed in Table 2 are shown in Fig. 6.

The data show that for a given exposure time the concentration of hydrogen is highest in the thinnest samples. At 397 days, the thickest sample (2.3 mm) has 68 wt ppm of hydrogen, the 1.0 mm thick sample has 146 wt ppm of hydrogen, and the 0.4 mm thick sample has 369 wt ppm of hydrogen, demonstrating hydrogen concentration correlates with the volume of the corrosion coupons. Furthermore, it is clear that the separation in weight gain observed between samples of different thicknesses also correlates with hydrogen content.

As previously addressed, corrosion data also exists for Zircaloy-4 with 130 ppm, 300 ppm, and 480 ppm additions of Ni (standard Zircaloy-4 only contains impurity amounts of Ni). Fig. 7 shows the weight gain of these samples versus corrosion time in 360 °C water for two sample thickness, 0.4 mm (purple) and 1.0 mm (green), again compared to the weight gain results for Zircaloy-4 samples shown in Fig. 5. The addition of Ni is correlated with an increase in weight gain, being highest for 480 ppm Ni addition, then 130 ppm Ni, and then no Ni addition. Ni has been linked to higher hydrogen pickup, and if hydrogen concentration accelerates corrosion than a higher pickup would lead to a faster acceleration of the corrosion rate [34]. The Zircaloy-4 with 130 ppm addition of Ni does not deviate much from the Zircaloy-4, however, as can be seen by the thinnest sample (purple), eventually the effect of the concentration of hydrogen begins to take over.

Fig. 8 shows the early weight gain behavior of these coupons plotted for both of the Zircaloy-4 ingots (see Table 1 for composition: Sn content varied by 0.07 wt% and Cr content varied by 0.02 wt%). Measurement uncertainty is less than 0.3 mg/dm^2, i.e. smaller than the data markers. A difference in weight gain appears at approximately the 2nd transition, whereas prior to this the corrosion weight gain is the same for all samples.

An increase in hydrogen concentration correlates with increasing weight gain of the samples and it appears that the

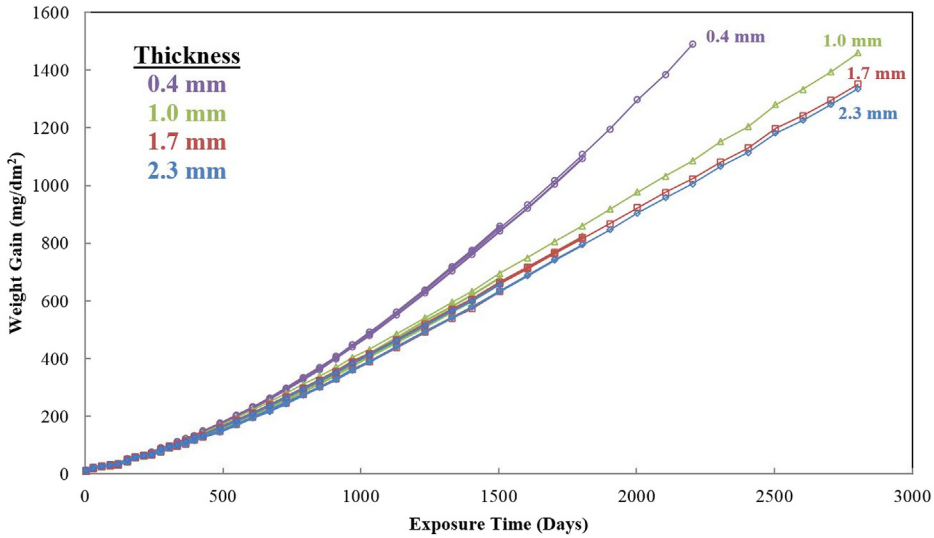

Fig. 5. Weight gain versus time plot of Zircaloy-4 coupons corroded in 360 °C water. Note that the weight gain of these identically exposed coupons depends on coupon thickness.

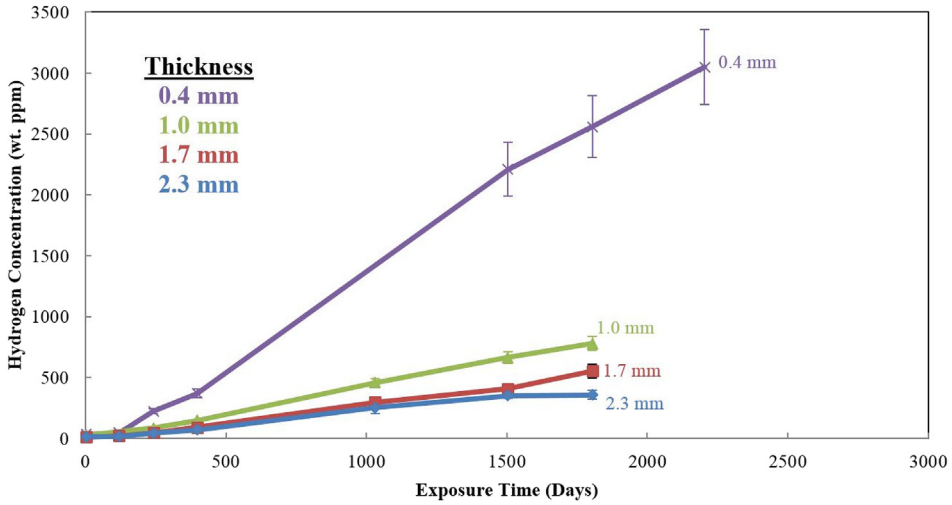

Fig. 6. Hydrogen concentration (in wt. ppm) measured with LECO hot vacuum extraction as a function of exposure time in autoclave at 360 °C water for Zircaloy-4 corrosion coupons of various thicknesses.

concentration of hydrogen in the thinnest sample at around the 2nd transition is sufficient to cause accelerated corrosion. Fig. 9 (a) shows the average time to transition for the samples with different thicknesses. Although all samples reach the first transition at the same time, the thinner samples start to reach transition at earlier and earlier times as hydrogen content increases, as shown in Fig. 9 (b). The amount of corrosion at the 2nd transition leads to a hydrogen concentration that exceeds the TSS for the thinnest (0.4 mm) samples. After reaching TSS (Fig. 9b) the coupons begin to transition earlier (Fig. 9a). Although some variability is seen due to ingot chemistry, the thinnest coupons clearly reach second transition in a shorter time than needed for the first transition once TSS is reached (after having reached the first transition at the same time as the other coupons).

Fig. 10 shows that the separation of the corrosion behavior of thick and thin corrosion coupons occurs when the hydrogen concentration is greater than the TSS. This suggests that the corrosion acceleration is related to the precipitation of hydrides in the metal, as the onset of the increased corrosion rate correlates with hydrogen concentration above the TSS of the alloy.

Fig. 11 shows the corrosion rate (mg/dm^2/day) versus exposure time. Only the samples tested for hydrogen concentration are included in this plot. Corrosion rate is calculated as the change in weight gain divided by the time step. The thinnest coupons clearly exhibit a higher corrosion rate than the thicker coupons. It is also noticeable that, after the initial ups and downs, the corrosion rate for the thinnest samples continues to increase with exposure time (and hydrogen concentration).

Fig. 12 best illustrates the dependence of corrosion on hydrogen content, by plotting corrosion rate (mg/dm^2/day) versus hydrogen content. The figure clearly shows that an increase in hydrogen content correlates with an increase in corrosion rate.

Fig. 13 compares these data to literature values for the corrosion rate of Zircaloy-4 samples with normal processing (commercial standard heat treatments) and which have undergone sufficient corrosion time to demonstrate post-transition corrosion rates. Kido et al. data were taken from Fig. 3, but since a relative post-transition corrosion rate (to non-hydrogen charged samples) was used, for comparison purposes this was set to the 0 ppm hydrogen value in Fig. 13 [12]. Additionally, the Kido et al. data were reported as initial hydrogen concentration, therefore, a final hydrogen concentration would shift those points to the right, more in line with the data reported in Fig. 13 [12]. The literature data also show an increase of corrosion rate in Zircaloy-4 with increasing hydrogen content, falling close to the data for Fig. 13.

To investigate the oxide morphology in order to understand why increasing hydrogen concentrations above the TSS results in higher corrosion rates, the samples were characterized using a fatigue fracture technique and subsequent SEM imaging. The fracture of the samples listed in Table 3 highlights the different microstructure and morphology of the oxide formed on samples with high hydrogen compared to those with low hydrogen. Fig. 14 shows two SEM micrographs of Zircaloy-4 samples with two different concentrations of hydrogen, 370 wt ppm on the left and 2560 wt ppm on the right.

Fig. 14 clearly demonstrates the microscopic differences between the oxide layer morphology in samples with low and high hydrogen content, namely the columnar versus equiaxed grain structure. As is clear in the sample 56038, on the left, (370 wt ppm H) the oxide forms long columnar grains. As hydrogen content increases, the oxide exhibits an evolution in morphology. The oxide grains become more equiaxed and less columnar. This is particularly evident when going from 370 wt ppm, left image, to 2560 wt ppm, right image, in Fig. 14. This morphology change could be interpreted either as a result or a cause of higher corrosion rate, but in any case, it is associated with this phenomenon.

Fig. 15 shows an SEM micrograph of Zircaloy-4 sample (100032) corroded in autoclave for 1804 days (54.9 μm average oxide thickness and 779 wt ppm H) demonstrating a mesoscopic view of the oxide and metal. In Fig. 15, the oxide shows a much more brittle fracture surface than the metal. The oxide transition layers can be clearly seen, as evidenced by the layer of cracks within the oxide. At this magnification, it is difficult to tell the difference hydrogen makes on the oxide morphology. It is possible, with a degree of uncertainty, to estimate the spacing between each transition layer and how this changes towards the metal-oxide interface. Rudimentary measurements appear to show that the spacing between transition layers decreases with increasing hydrogen content.

Qualitatively, examination of crack spacing can be used to determine oxide transition layer thickness. In a heavily hydrided sample, not shown, (2560 wt ppm H) there is a progression from larger transition spacing near the oxide-water interface (first to form) to a smaller transition spacing as one moves toward the metal-oxide interface. The change in crack spacing is difficult to

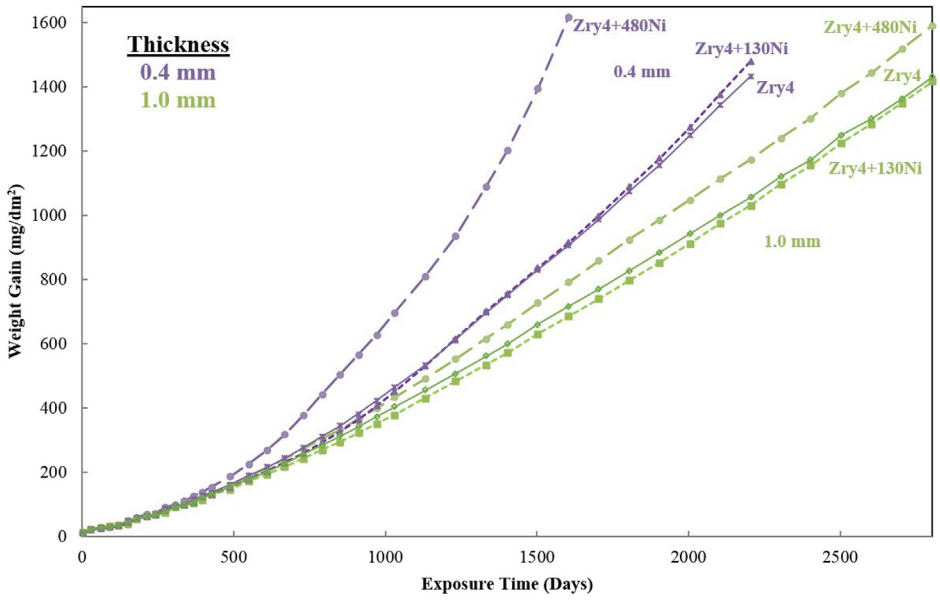

Fig. 7. Comparison of Zircaloy-4+130 ppm Ni (dotted lines), Zircaloy-4+480 ppm Ni (dashed lines), and Zircaloy-4 (solid lines) weight gain data for the two thinnest coupon groups demonstrating the effect of additional Ni on corrosion behavior, likely due to increased hydrogen pickup.

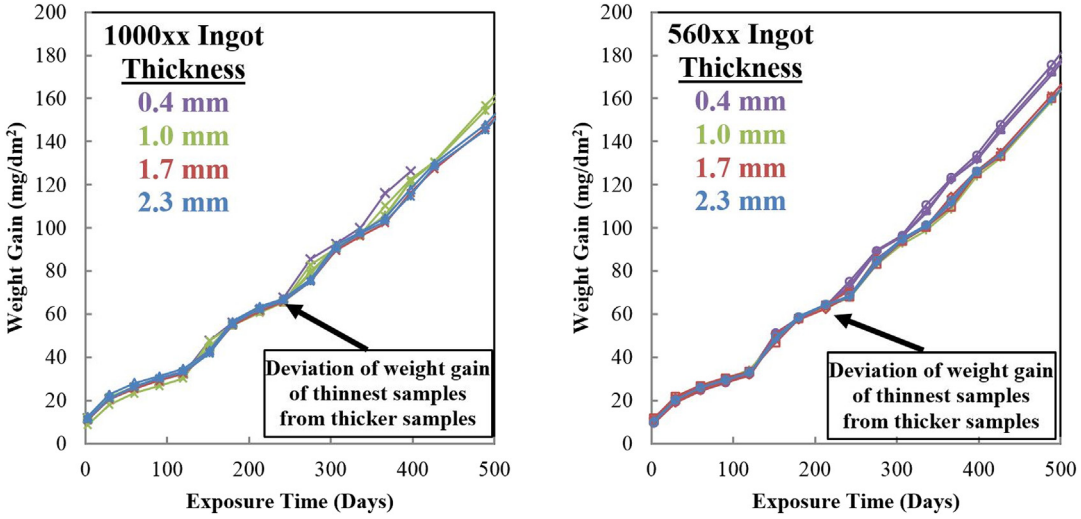

Fig. 8. Early weight gain of Zircaloy-4 in 360 °C water separated by ingot, 1000xx (left) and 560xx (right). These plots show that the dependence of weight gain on coupon thickness begins to appear around the second transition.

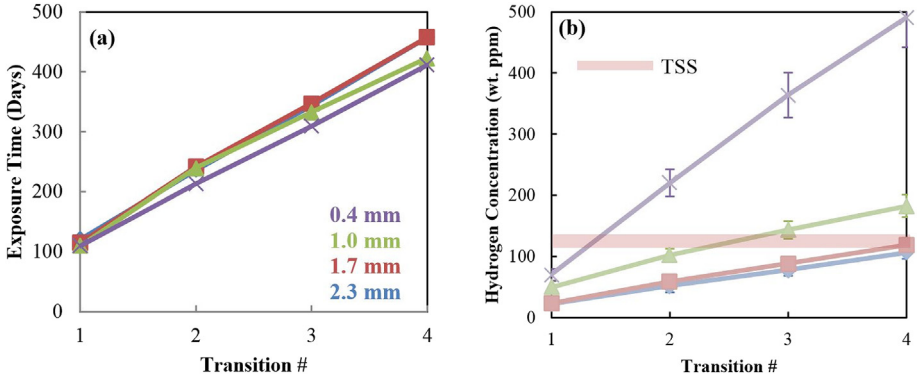

Fig. 9. The amount of total corrosion time to each transition as a function of transition number, left, with the hydrogen concentration at each transition number, right, for 360 °C autoclave corrosion coupons. After reaching TSS the coupons begin to transition earlier.

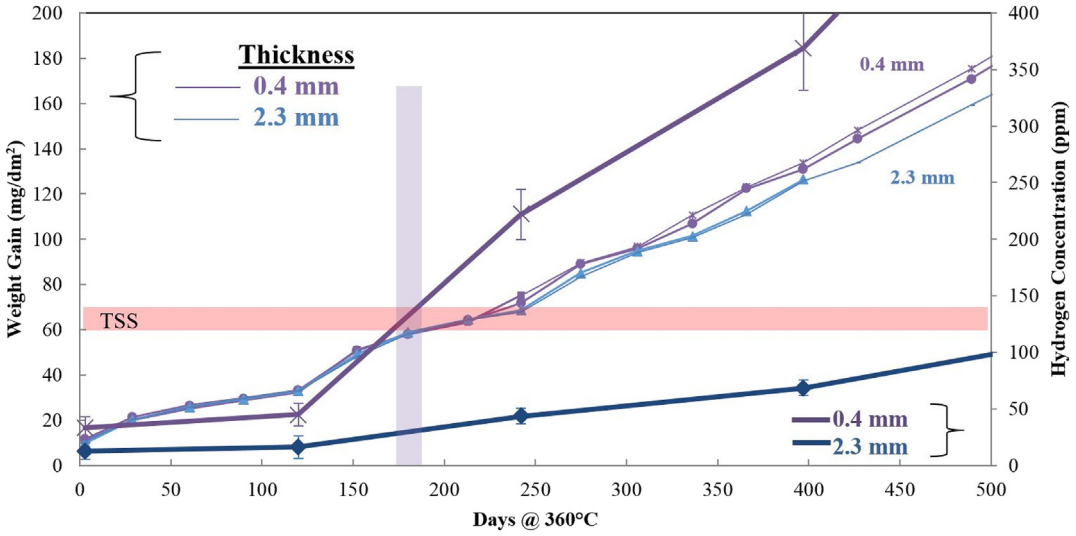

Fig. 10. Overlay of TSS_d values [5–10] (red bar) with the weight gain (thin lines in mg/dm^2) and hydrogen concentration (thick lines in ppm) which illustrate in Zircaloy-4 samples where the onset of the accelerated corrosion in the thinnest coupons occurs (just after crossing TSS-purple bar). (For interpretation of the references to colour in this figure legend, the reader is referred to the web version of this article.)

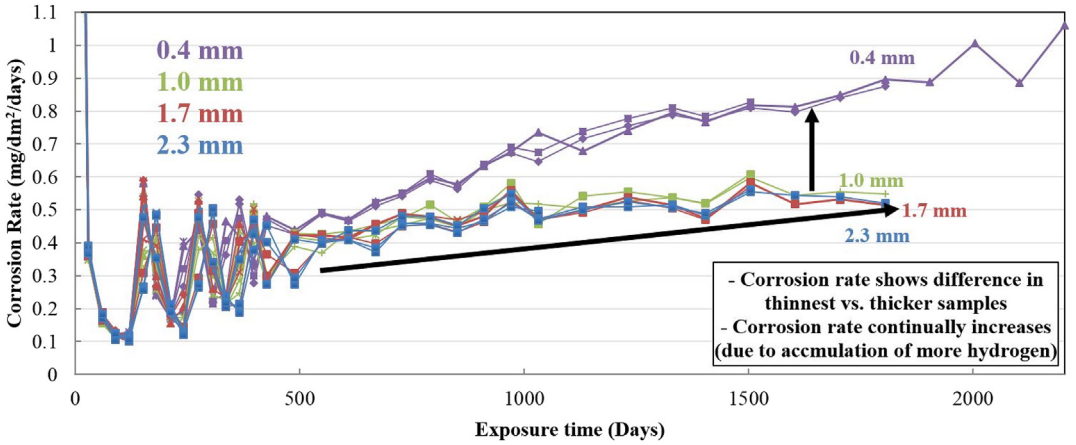

Fig. 11. Corrosion rate vs. time for 360 °C Zircaloy-4 autoclave corrosion coupons, showing higher corrosion rates for thinner coupons later in life.

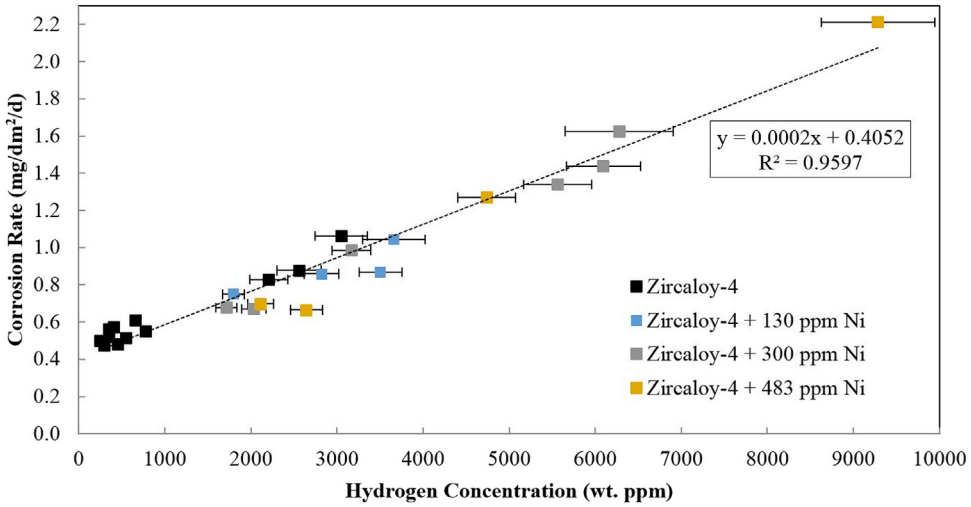

Fig. 12. Post-transition corrosion rate as a function of hydrogen concentration (wt. ppm) for Zircaloy-4360 °C autoclave corrosion coupons with hydrogen concentrations measured with LECO hot vacuum extraction. All hydrogen concentrations are above the TSS and values of corrosion rate are shown where it was possible to determine a post-transition corrosion rate.

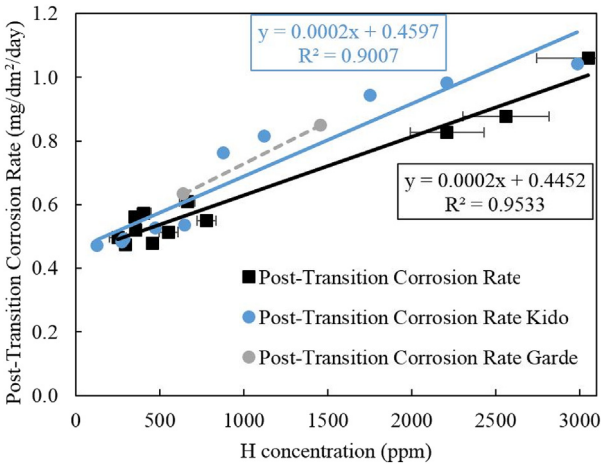

Fig. 13. Post-transition corrosion rate versus hydrogen concentration with data from Fig. 12 compared to literature values [12] [13]. Reasonable agreement is shown between literature data and data collected in this study.

determine given the fracture and uneven surface, but is estimated to decrease by 10–15% from the first oxide formed to the oxide formed nearest the metal-oxide interface. This indicates that Zircaloy-4 is reaching transitions faster with more hydrides, consistent with analysis of weight gain and hydrogen data above.

Hydrides can precipitate near grain boundaries at the metal-oxide interface amongst other locations. Fig. 16 shows an SEM micrograph of an oxide layer formed on a Zircaloy-4 sample corroded at 360 °C for 1804 days. The oxide advance is greater where the hydrides appear to intersect the metal-oxide interface. This increased hydriding could be a cause or an effect of the higher corrosion rate.

The degree of oxide penetration into the metal where hydrides are located is greater in materials with higher hydrogen concentration. This leads to a more uneven metal-oxide interface, as shown in Fig. 17 with three SEM micrographs, on the same scale, of Zircaloy-4 samples with (a) 664 wt ppm H, (b) 3050 wt ppm H, and (c) 2210 wt ppm H. The samples with higher hydrogen contents (b) and (c) have a rougher interface than the sample with lower hydrogen content (a). The increase in the length of the metal-oxide interface over a constant horizontal width is ~15% from Fig. 17 (a) to (b). This corresponds to an increase in the surface area of the metal-oxide interface of approximately 33%. An increased surface area of the metal-oxide interface will lead to a higher corrosion rate due to the increased area where the oxygen can access the metal.

4. Discussion

The evidence shown in Fig. 5 demonstrates that thinner coupons exhibit higher weight gains than thicker coupons from the same starting ingot despite identical initial processing and environmental exposure. Although this difference is particularly evident near the end of the autoclave exposure times and for the thinnest specimens, this differentiation in corrosion rate begins as early as the second transition cycle, as shown in Fig. 8. The data suggest that the accelerated corrosion in thinner coupons is associated with the onset of hydride precipitation. As can be seen in Fig. 10, corrosion of the thinner samples begins to diverge from that of thicker samples upon reaching the TSS_d value for Zircaloy-4 at 360 °C (shown as ranging from 120 to 140 wt ppm). Fig. 9 also shows that coupons that reach the TSS begin to undergo kinetic transitions at earlier times in the autoclave, although, it should be noted that the precision of determination of the transition time is limited by the frequency of weight gain measurements.

The increase in corrosion rate is also associated with the onset of hydride precipitation, as shown in Fig. 11. It is clear that thinner coupons have higher corrosion rates. Fig. 12 clearly shows that the post-transition corrosion rate increases with increasing hydrogen concentration (correlating linearly). This would support the idea that an increased hydride concentration leads to faster corrosion. If, as Figs. 16 and 17 suggest, the oxide layer preferentially corrodes in locations where hydrides are located, then it would follow that more hydrides would favor faster corrosion.

Other effects of hydrogen ingress are less likely to change the corrosion rate of Zr alloys [18,30,35,36]. Although hydrogen dilates the matrix (1% volume per 1000 ppm H) the resolved strains are relatively small and would act to relax stresses rather than increase them [35]. It is possible that hydrogen affects the creep rate of Zircaloy-4 either in solid solution (increase creep rate) or as hydrides (decrease creep rate); however, these possibilities have not been examined here [37]. The strain exerted by the oxide on the metal would be more significant for thinner samples, but the protective, adherent part of the oxide (maximum of ~3 μm) is small compared to the metal thickness, so that the stress induced on the thinnest sample with the thickest oxide would be not be significant. Furthermore, given that the observed increase in corrosion rate is first observed at only a few microns of oxide growth (as demonstrated in Fig. 8), the strain rate at this point would be insufficient to accelerate the corrosion.

Given the observations, there are a few possibilities for the observed enhancement of corrosion by hydrogen. (1) It is possible that hydrides harden the metal matrix ahead of the oxide front, thus making it more difficult for the metal to deform plastically and relax any accumulated stresses in the oxide layer. The lessened

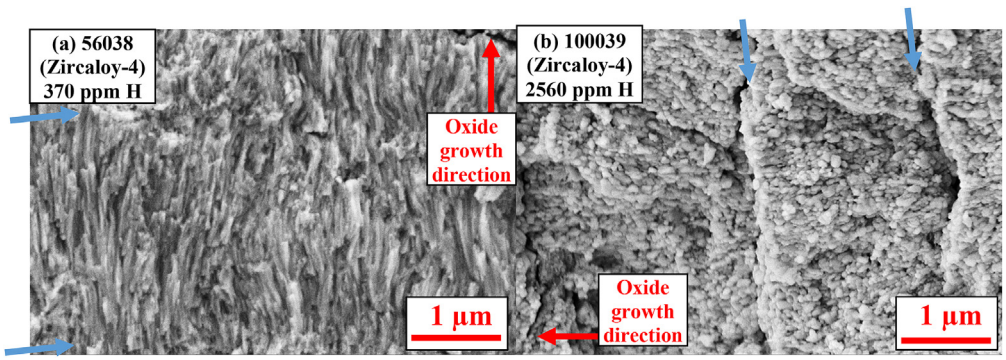

Fig. 14. SEM images of 0.4 mm thick Zircaloy-4 coupons corroded for 397 days, (8.7 μm, 370 wt ppm hydrogen, left) and 1804 days, (71.6 μm, 2560 wt ppm hydrogen, right) in autoclave at 360 °C. Locations of transition cracks are shown with blue arrows. (For interpretation of the references to colour in this figure legend, the reader is referred to the web version of this article.)

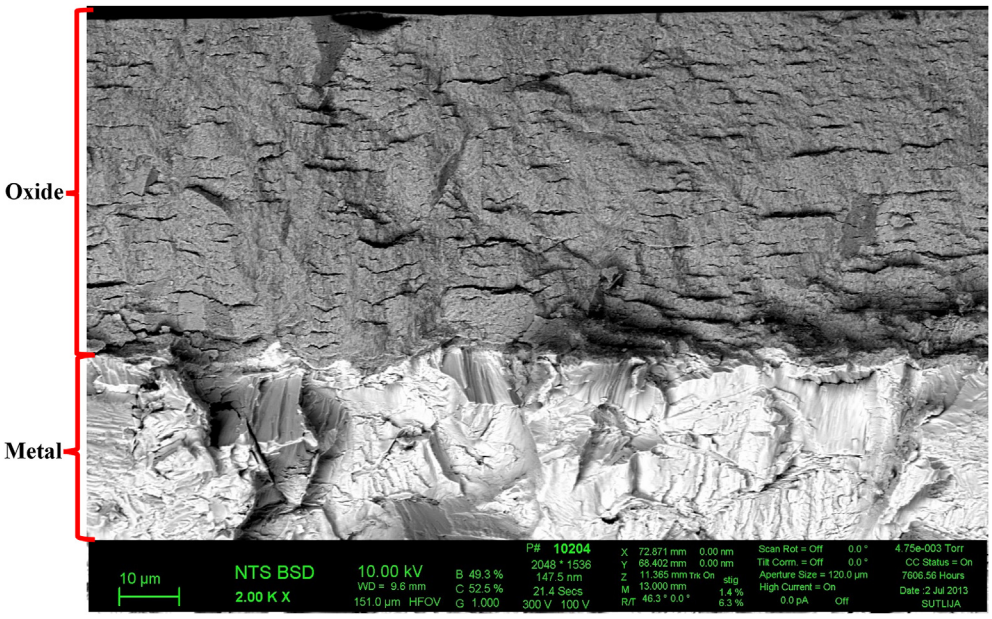

Fig. 15. SEM image of a fatigue fractured Zircaloy-4360 °C autoclave corrosion coupon 100032, 779 wt ppm H.

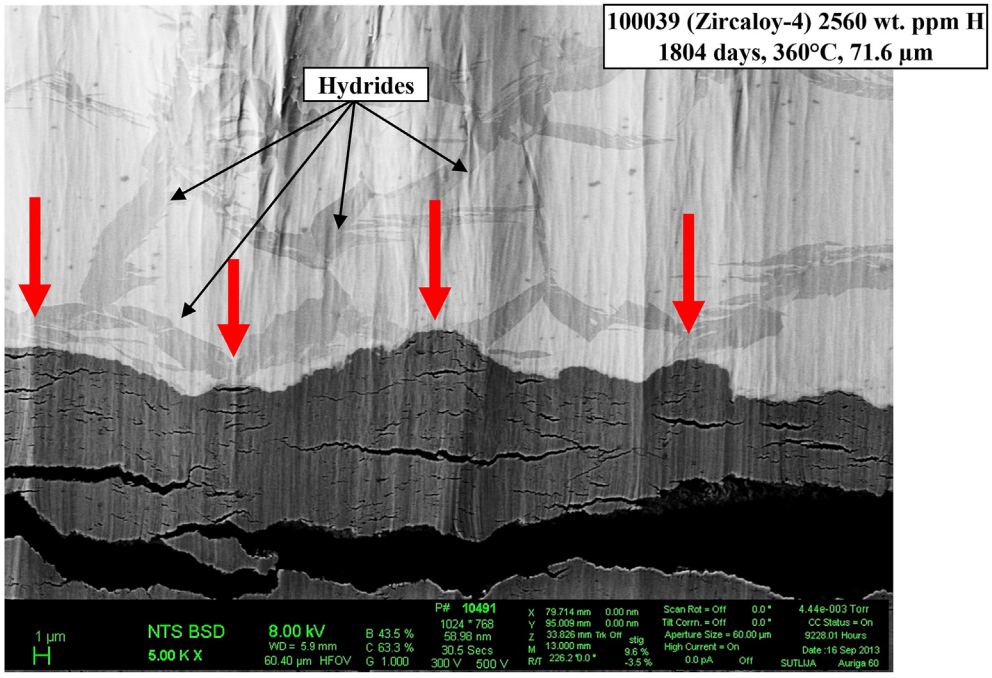

Fig. 16. SEM micrograph of Zircaloy-4 sample 100039 corroded for 1804 days at 360 °C (71.6 µm). The oxide growth was accelerated along locations of hydrides, as highlighted with red arrows. (For interpretation of the references to colour in this figure legend, the reader is referred to the web version of this article.)

ability of the metal to plastically deform would then lead to earlier breaking of the oxide layer (earlier transition). Fig. 9 shows evidence of earlier transitions occurring in the samples with hydrogen concentrations above the TSS. (2) Figs. 16 and 17 show an uneven metal-oxide interface caused by the oxide growth in areas of the metal where hydrides are located. The increase in the uneven oxide growth leads to a larger surface area of the metal-oxide interface. This larger surface area in the samples with increased hydrogen concentration (estimated in Fig. 17 to be ~33%) gives more access to oxidizing species to the metal, thus leading to a higher observed uniform corrosion rate. It is hypothesized that (1) and (2) lead to the observed increase in corrosion rate of samples with increased hydrogen concentration. A compounding effect is that research has shown that as transition is approached, the interface becomes more uneven and that this causes higher stresses, which could also lead to earlier transitions [38,39].

These two observations support the hypothesis that the hydride presence in the metal ahead of the oxide front causes accelerated corrosion in zirconium alloys. It is not yet possible to determine if the oxide structure (seen in Fig. 14) formed in the hydrided samples is a cause or a consequence of the accelerated oxide growth, but it is correlated with higher hydrogen contents. It is also possible that

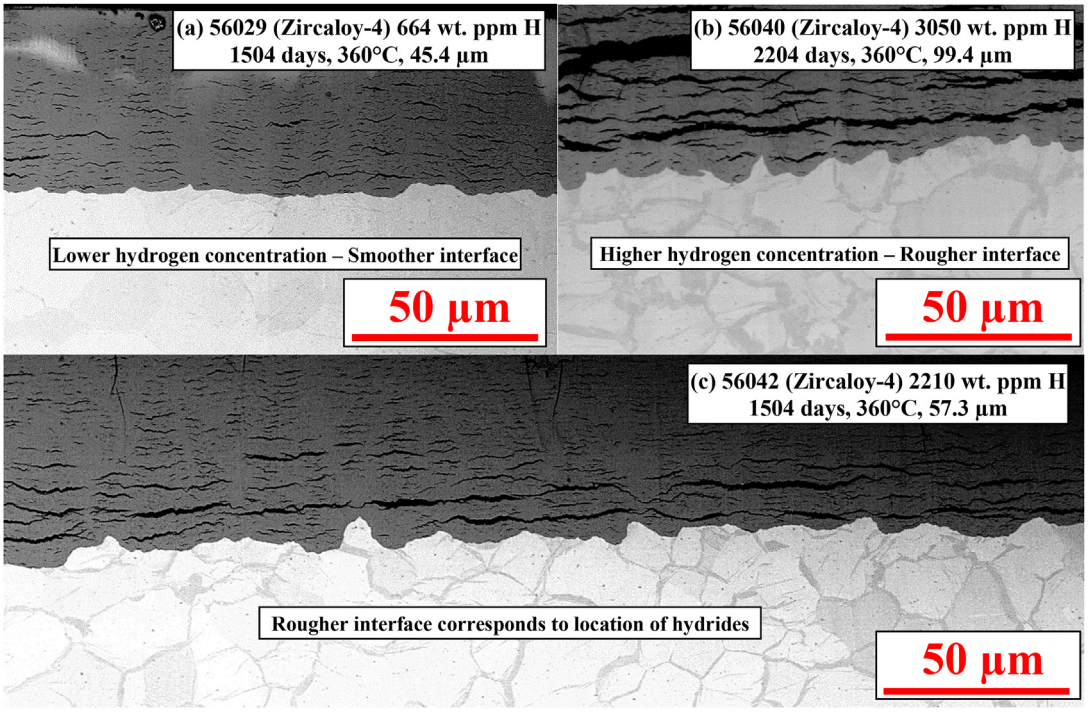

Fig. 17. Comparison of SEM micrographs of three Zircaloy-4 samples corroded at 360 °C with varying hydrogen concentrations. The higher the concentration of hydrogen, the more uneven the oxide growth was at the metal-oxide interface, related to the presence of the hydrides in the metal.

the fracture test of samples with more hydrides in the metal (and thus more brittle) does not adequately preserve the oxide grain structure. The observation that there are more frequent transitions could mean that thresholds for mechanical breakdown of the oxide layer are reached sooner, thus accelerating corrosion. More research is still needed to determine the mechanism by which increased hydrogen content accelerates corrosion.

One could expect then that corrosion testing material that has a higher level of cold work would lead to similar hardening of the metal and therefore could be used as an analog to test this hypothesis. Although research of the effect of cold work on zirconium alloy corrosion has been performed, a systematic investigation of this phenomenon is still lacking [40,41,42,43,44].

5. Conclusions

A systematic study was conducted to determine the effect of hydrogen concentration in Zircaloy-4 and Zircaloy-4 with Ni additions on the corrosion rate. The samples had the same process of hydrogen absorption as occurs during corrosion (no pre-charging). Samples were corroded at 360 °C in a water autoclave and were fabricated with different thicknesses, which in turn gives a range of hydrogen concentrations. Periodic weight gain measurements were combined with hydrogen concentration measurements and fatigue fracture of samples with subsequent SEM imaging to corroborate and interpret the findings. The conclusions from this study are as follows:

- Hydrogen concentrations above the TSS (formation of hydrides) are associated with accelerated zirconium alloy corrosion, so that higher hydrogen concentrations lead to higher corrosion rates.
- As hydrogen concentration increases above the TSS, it appears that periodic oxide transitions occur earlier.
- Increased hydride concentration is associated with a change in oxide layer morphology from long columnar to more equiaxed grains.
- Regions of advanced oxide growth into the metal were associated with the locations of precipitated hydrides near the metal-oxide interface.
- It is hypothesized that local hardening of the metal matrix where hydrides are located causes the metal to be less able to accommodate oxide growth stresses and leads to earlier oxide kinetic transitions. This leads to a more uneven metal-oxide interface, which increases the surface area between the metal and the oxide, which in turn increases the access of oxidizing species to the metal leading to increased observed corrosion rates.

Acknowledgements

Many people were involved in the work in this report, certainly more than is possible to acknowledge; however, the authors would like to thank the following engineers, scientists, and technicians for their contributions. Ken Bousman (LECO) and Bruce Kallenburg (fatigue fracture) for their work. The various report and model authors and past test sponsors all deserve acknowledgement, but particularly H. Richard Peters, Karen Roarty-Dansfield, and Dale Taylor. This research was performed (B. Ensor) under appointment to the Rickover Fellowship Program in Nuclear Engineering sponsored by Naval Reactors Division of the U.S. Department of Energy.

References

[1] C. Lemaignan, A.T. Motta, Zirconium alloys in nuclear applications, in: B. Frost (Ed.), Materials Science and Technology, a Comprehensive Treatment, 10B, VCH, 1994, pp. 1–51.
[2] B.F. Kammenzind, D.G. Franklin, H.R. Peters, W.J. Duffin, Hydrogen pickup and redistribution in alpha-annealed Zircaloy-4, in: Zirconium in the Nuclear Industry: Eleventh International Symposium, ASTM STP 1295, 1996, pp. 338–370.

[3] A. Couet, A.T. Motta, R.J. Comstock, Hydrogen pickup measurements in zirconium alloys: relation to oxidation kinetics, J. Nucl. Mater. 451 (2014) 1–13.
[4] A. Couet, A.T. Motta, R.J. Comstock, Effect of alloying elements on hydrogen pickup in zirconium alloys, in: Zirconium in the Nuclear Industry: 17th International Symposium, ASTM STP 1543, 2014, pp. 479–509.
[5] A.T. Motta, L.-Q. Chen, Hydride formation in zirconium alloys, J. Metal 64 (12) (2012) 1403–1408.
[6] J.J. Kearns, Terminal solubility and partitioning of hydrogen in the alpha phase of zirconium, Zircaloy-2 and Zircaloy-4, J. Nucl. Mater. 22 (1967) 292–303.
[7] A. Sawatzky, B.J.S. Wilkins, Hydrogen solubility in zirconium alloys determined by thermal diffusion, J. Nucl. Mater. 22 (1967) 304–310.
[8] W.H. Erickson, D. Hardie, The influence of alloying elements on the terminal solubility of hydrogen in alpha-zirconium, J. Nucl. Mater. 13 (1964) 254–262.
[9] A. McMinn, E.C. Darby, J.S. Schofield, The terminal solid solubility of hydrogen in zirconium alloys, in: Zirconium in the Nuclear Industry: Twelfth International Symposium, ASTM STP 1354, 2000, pp. 173–195.
[10] K. Une, S. Ishimoto, Dissolution and precipitation behavior of hydrides in Zircaloy-2 and high Fe Zircaloy, J. Nucl. Mater. 322 (2003) 66–72.
[11] M.P. Puls, The effects of misfit and external stresses on terminal solid solubility in hydride-forming metals, Acta Metall. 29 (1981) 1961–1968.
[12] T. Kido, K. Kanasugi, M. Sugano, K. Komatsu, PWR Zircaloy cladding corrosion behavior: quantitative analyses, J. Nucl. Mater. 248 (1997) 281–287.
[13] A.M. Garde, Enhancement of aqueous corrosion of Zircaloy-4 due to hydride precipitation at the metal-oxide interface, in: Zirconium in the Nuclear Industry: Ninth International Symposium, ASTM STP 1132, 1991, pp. 566–594.
[14] M. Blat, D. Noel, Detrimental role of hydrogen on the corrosion rate of zirconium alloys, in: Zirconium in the Nuclear Industry: Eleventh International Symposium, ASTM STP 1295, 1996, pp. 319–337.
[15] M. Tupin, C. Bisor, P. Bossis, J. Chene, J.L. Bechade, F. Jomard, Mechanism of corrosion of zirconium hydride and impact of precipitated hydrides on the Zircaloy-4 corrosion behaviour, Corros. Sci. 98 (2015) 478–493.
[16] P. Bossis, B. Verhaeghe, S. Doriot, D. Gilbon, V. Chabretou, A. Dalmais, J.-P. Mardon, M. Blat, A. Miquet, In PWR comprehensive study of high burn-up corrosion and growth behavior of M5 and recrystallized low-tin Zircaloy-4, J. ASTM Int. 6 (2) (2009) 1–27.
[17] D.M. Rishel, B.F. Kammenzind, The role of gamma radiation on Zircaloy-4 corrosion, in: 18th International Symposium on Zirconium in the Nuclear Industry, ASTM STP 1597, May 2016.
[18] P. Platt, E. Polatidis, P. Frankel, M. Klaus, M. Gass, R. Howells, M. Preuss, A study into stress relaxation in oxides formed on zirconium alloys, J. Nucl. Mater. 456 (2015) 415–425.
[19] M. Billone, Y. Yan, T. Burtseva, R. Daum, Cladding Embrittlement during Postulated Loss-of-coolant Accidents, 2008. NRC Doc. No NUREG/CR-6967.
[20] M. Blat, L. Legras, D. Noel, H. Amanrich, Contribution to a better understanding of the detrimental role of hydrogen on the corrosion rate of Zircaloy-4 cladding materials, in: Zirconium in the Nuclear Industry: Twelfth International Symposium, ASTM STP 1354, 2000, pp. 563–591.
[21] T. Kido. A Study on Enhanced Uniform Corrosion of Zircaloy-4 Cladding During High Burnup Operation in PWRs, in: Sixth International Symposium on Environmental Degradation of Materials in Nuclear Power Systems, San Diego, Aug. 1-5, 1993.
[22] Y.-S. Kim, Y.-H. Jeong, S.-B. Son, A study of the effects of dissolved hydrogen on zirconium alloys corrosion, J. Nucl. Mater. 444 (2014) 349–355.
[23] A.T. Motta, M.J.G. da Silva, A. Yilmazbayhan, R.J. Comstock, Z. Cai, B. Lai, Microstructural characterization of oxides formed on model Zr alloys using synchrotron radiation, J. ASTM Int. 5 (3) (2008) 1–20. JAI101257.
[24] B. Cox, Some thoughts on the mechanisms of in-reactor corrosion of zirconium alloys, J. Nucl. Mater. 336 (2005) 331–368.
[25] B. Ensor, The Nature of Unstable Oxide Growth in Zirconium and Zirconium Alloys, PhD Thesis in Nuclear Engineering, The Pennsylvania State University, 2016.
[26] B.F. Kammenzind, J.A. Gruber, R. Bajaj, J.D. Smee, Neutron irradiation effects on the corrosion of Zircaloy-4 in a PWR environment, in: 18th International Symposium on Zirconium in the Nuclear Industry, ASTM STP 1597, May 2016.
[27] B.V. Cockeram, L. K.J, T. Byun, L. Snead, J. Hollenbeck, Development of microstructure and irradiation hardening of Zircaloy during low dose neutron irradiation at nominally 377-440C, J. Nucl. Mater. 449 (2014) 69–87.
[28] R. Bajaj, B.F. Kammenzind, D. Farkas, Effects of neutron irradiation on the microstructure of alpha-annealed Zircaloy-4, in: Zirconium in the Nuclear Industry: Thirteenth International Symposium, ASTM STP 1423, 2002, pp. 400–426.
[29] B.V. Cockeram, K. Chan, In situ studies and modeling the fracture of Zircaloy-4, J. Nucl. Mater. 393 (2009) 387–408.
[30] B.F. Kammenzind, K. Eklund, R. Bajaj, The influence of in-situ clad straining on the corrosion of Zircaloy in a PWR water environment, in: Zirconium in the Nuclear Industry: Thirteenth International Symposium, ASTM STP 1423, 2002, pp. 524–560.
[31] K. Anderson, R. Bajaj, Microstructural and microchemical analyses of extracted second-phase precipitates in alpha-annealed and beta-quenched Zircaloy-4, Microsc. Microanal. 20 (Suppl 3) (2014) 500–501.
[32] ASTM, Standard E1820-11: Standard Test Method for Measurement of Fracture Toughness, ASTM International, West Conshohocken, PA, 2011.
[33] ASTM, Standard E399-12: Standard Test Method for Linear-elastic Plane-strain Fracture Toughness Klc of Metallic Materials, ASTM International, West Conshohocken, PA, 2012.
[34] A.P. Shivprasad, A.T. Motta, A. Kucuk, S. Yagnik, Z. Cai. Microbeam X-ray absorption near-edge spectroscopic studies of high-burnup Zircaloy-2 oxide layers, in: 18th International Symposium on Zirconium in the Nuclear Industry ASTM STP 1597, 17th May 2016.
[35] M. Blat-Yrieix, A. Ambard, F. Foct, A. Miquet, S. Beguin, N. Cayet, Toward a better understanding of dimensional changes in Zircaloy-4: what is the impact induced by hydrides and oxide layer?, in: Zirconium in the Nuclear Industry: 15th International Symposium, ASTM STP 1505, 2009, pp. 594–611.
[36] P. Barberis, V. Rebeyrolle, J. Vermoyal, V. Chabretou, J. Vassault, CASTA DIVA(R): experiments and modeling of oxide-induced deformation in nuclear components, in: Zirconium in the Nuclear Industry: 15th International Symposium, 2009, pp. 612–631.
[37] Y.-I. Jung, Y.-N. Seol, B.-K. Choi, J.-Y. Park, Thermal creep of Zircaloy-4 tubes containing corrosion-induced hydrogen, J. Nucl. Mater. 419 (2011) 213–216.
[38] P. Platt, S. Wedge, P. Frankel, M. Gass, R. Howells, M. Preuss, A study into the impact of interface roughness development on mechanical degradation of oxides formed on zirconium alloys, J. Nucl. Mater. 459 (2015) 166–174.
[39] P. Platt, P. Frankel, M. Gass, M. Preuss, Critical assessment of finite element analysis applied to metal-oxide interface roughness in oxidising zirconium alloys, J. Nucl. Mater. 464 (2015) 313–319.
[40] I.A. El-Shanshoury, V.A. Rudenko, M.E. El-Dahshan, The effect of cold-work on the oxidation of Zr-1%Nb alloy in air and pressurized steam at 450-550 C, Corros. Sci. 9 (1969) 479–488.
[41] D. Charquet, Improvement of the uniform corrosion resistance of Zircaloy-4 in the absence of irradiation, J. Nucl. Mater. 160 (1988) 186–193.
[42] Y.H. Jeong, K.S. Rheem, H.M. Chung, Characteristics of autoclave and in-reactor nodular corrosion of zircaloys, in: Zirconium in the Nuclear Industry: Ninth International Symposium, ASTM STP 1132, 1991, pp. 683–717.
[43] D. Charquet, Microstructure and properties of zirconium alloys in the absence of irradiation, in: Zirconium in the Nuclear Industry: Twelfth International Symposium, ASTM STP 1354, 2000, pp. 3–14.
[44] V.F. Urbanic, M. Griffiths, Microstructural aspects of corrosion and hydrogen ingress in Zr-2.5Nb, in: Zirconium in the Nuclear Industry: Twelfth International Symposium, ASTM STP 1354, 2000, pp. 641–657.